KFUPM
Journal of Undergraduate Research International

Diamond Open Access 163

Article Mechanical Engineering

System-Level Analysis of a DCMD and PEMWE Integrated System for Hydrogen and Water Cogeneration

Alaa M. Ahmed and Atia E. Khalifa*

Cite https://doi.org/10.64589/juri/231609

Submitted: April 24, 2026 **Revised:** May 17, 2026 **Accepted:** May 21, 2026

ABSTRACT

The integration of desalination and hydrogen production offers a promising pathway to simultaneously address water scarcity and clean energy demands. This study evaluated the feasibility and performance of coupled direct contact membrane distillation (DCMD) and proton exchange membrane water electrolyzer (PEMWE) systems for water–hydrogen cogeneration. A validated steady-state model was developed, incorporating coupled heat and mass transfer in DCMD and electrochemical, thermal, and hydrogen production models for PEMWE. A parametric analysis was conducted under two operational scenarios: (i) full coupling with zero net water output, and (ii) cogeneration of freshwater and hydrogen. The results indicate that system operation is constrained by the balance between DCMD production and PEMWE consumption, yielding a maximum current density of 2.29 A/cm^2 for a 50 cm^2 (1–2 kW) electrolyzer supported by a 200 cm^2 DCMD membrane. The net water production decreased from approximately 0.70 kg/h at zero current density to zero at this limit. The system efficiency decreased with increasing current density owing to rising activation and ohmic losses, as well as higher cooling requirements. By contrast, increasing stack temperature from 50 to 80 °C reduced cell voltage and improved overall efficiency, while lowering cooling demand. The feed temperature strongly enhanced the DCMD productivity, enabling higher feasible operating current densities. In the cogeneration mode, increasing the membrane area to 0.5 m^2 enabled simultaneous operation, with more than 95% of the produced water remaining available as useful output. These findings provide design insights for the development of water-efficient green hydrogen systems, particularly for deployment in water-limited regions.

Keywords: water desalination, membrane distillation, PEMWE, hydrogen production, integrated system, performance analysis

1. INTRODUCTION

Given the rising energy demand, hydrogen has gained increasing attention as a key energy carrier for decarbonization owing to its high gravimetric energy density and zero-emission combustion [1]. However, most hydrogen is currently produced from fossil fuels, resulting in significant greenhouse gas emissions [2]. One of the most prominent methods for green hydrogen production is electrolysis, in which hydrogen is generated by splitting water using electricity [3]. The proton exchange membrane water electrolyzer (PEMWE) is a leading technology for generating high-purity green hydrogen because its rapid response capability allows it to effectively manage the fluctuating power output of intermittent renewable energy sources [3]. Despite its technical advantages, this system is exceptionally sensitive to water quality and requires an ultrapure water supply to prevent system degradation [4]. ASTM International recommends the use of Type I deionized water for proton exchange membrane (PEM) electrolysis [5]. Stoichiometrically, electrolysis requires approximately 9 kg water to produce 1 kg hydrogen [6]. However, in practice, more water is required owing to the cooling requirements and system losses [6]. Of significant concern, over one-third of the existing and planned low-carbon hydrogen facilities are in regions experiencing significant water scarcity [7]. Various approaches have been proposed to address the water demand for electrolysis, including direct seawater electrolysis [8], industrial wastewater utilization [9], and multiple desalination methods [10]. Desalination technologies can be classified into membrane-based methods, such as reverse osmosis (RO) and electrodialysis, and thermal-based methods, such as multistage flash and multi-effect distillation (MED) [11]. Owing to its maturity and scalability, most integrated desalination–electrolysis systems have focused on RO. Katakam et al. [12] studied the limitations of RO-based systems and showed that achieving ultrapure water standards is theoretically possible but requires a significant increase in the membrane area. Ellersdorfer et al. [13] developed a MATLAB-based numerical model of an integrated solar photovoltaic (PV)–RO–PEM system, incorporating both water purity and electrolyzer cooling demand. Their analysis also compared RO with MED and showed that MED can be more cost-effective when low-grade waste heat is available. Kianfard et al. [14] explored the integration of RO with PEM in a geothermal-powered multigeneration system for simultaneous hydrogen and water production. Nonetheless, RO typically produces water with total dissolved solids levels between 10

Published under an exclusive license by KFUPM

and 100 ppm, which is inadequate for PEM systems[15]. Consequently, RO–PEM configurations typically require an additional polishing step such as electrodeionization[15]. Furthermore, RO requires high pressures to overcome osmotic pressure, rendering it energy-intensive and unable to treat extremely high-salinity feedwater[11]. To address these limitations, PEM systems should consider alternative desalination methods, particularly membrane distillation (MD). MD is a thermally driven desalination process that separates water vapor from a hot saline feed stream through a hydrophobic membrane using a temperature-induced vapor-pressure gradient. MD operates at low temperatures and can be integrated with low-grade or waste heat, reducing energy consumption and improving sustainability. It offers a high rejection efficiency and effectively removes salts, contaminants, and microorganisms to produce high-purity water. In contrast to pressure-driven processes, MD requires a low operating pressure, which results in simpler equipment and reduced mechanical stress on the system. Additionally, its performance is less affected by high salinity, rendering it suitable for treating seawater and concentrated brine. Its compact and modular design allows easy scalability and flexibility in various applications, rendering it an attractive option for modern water treatment. One of the common MD configurations is direct contact membrane, where the membrane separates the hot saline feed stream from the cold permeate water stream. In direct contact MD (DCMD), vapor passes through a membrane and condenses directly in a cold permeate stream. Several studies have investigated the integration of electrolysis with MD. Arthur et al.[16] demonstrated the integration of an MD heat exchanger with a commercial 2.2 kW anion exchange membrane electrolyzer to evaluate simultaneous thermal management and water production. Xu et al.[17] utilized finite element modeling and Aspen Plus simulations to optimize an integrated system that coupled seawater MD with alkaline water electrolysis. Their results showed that the MD unit could achieve a sufficient water supply, exceeding the electrolyzer's demand. Schwantes et al.[18] utilized numerical simulations and laboratory experiments to assess the techno-economic feasibility of using permeate gap MD driven by waste heat from a 5 MW PEM electrolyzer. The study experimentally produced distillate with conductivity below 3 μS/cm and found that MD is approximately 40% more cost-efficient than RO for seawater desalination when leveraging the waste heat from the electrolyzer. Zhao et al.[19] experimentally demonstrated the feasibility of DCMD for purifying various water sources to meet PEM requirements, achieving distillate conductivities as low as 0.98 μS/cm. This study evaluated the use of waste heat from a PEM electrolyzer to heat a DCMD feed stream using a simplified model. While feasible, they suggested that a dedicated heater is still needed, with waste heat improving the overall efficiency.

In contrast to previous studies that mainly focused on the feasibility of MD for PEM water purification or waste-heat utilization, this study presents a comprehensive steady-state theoretical model of an integrated system combining DCMD and PEMWE, assuming PV power. The model evaluates the water production, PEM water requirements, hydrogen generation, and overall system efficiency. A parametric analysis was conducted to investigate the key factors governing system performance and integration. Two operational scenarios were considered: (i) DCMD water production was completely utilized by the PEM electrolyzer for hydrogen production, and (ii) DCMD was operated for the cogeneration of freshwater demand and hydrogen production. This study provides benchmark data for the system design and operation that may be used to enhance the system and optimize its performance.

The remainder of this paper is organized as follows. Section 2 describes the system and presents the fundamental equations governing the model. Section 3 presents and discusses the model validation results. Section 4 discusses the results for both operational scenarios and the study limitations. Finally, Section 5 concludes the paper with a summary of the main findings.

2. SYSTEM DESCRIPTION AND ASSUMPTIONS

2.1. System description. This section describes the integrated DCMD and PEM electrolysis systems shown in Figure 1. The DCMD unit receives heated saline feedwater from a hot feed tank and operates in a counter-flow configuration, where the permeate side is connected to a chilled freshwater tank. The heat and mass transfer across the membrane enable the production of purified water, which is collected in a chilled permeate tank. The permeate tank serves as the central integration point of the system. Water from the chilled permeate tank is supplied to both the DCMD permeate channel and PEM electrolyzer. Within the PEM system, a portion of the incoming water is consumed in the electrolysis reaction to produce hydrogen and oxygen, whereas the remaining water is recirculated into the permeate tank. The entire system is powered by solar PV panels. In this study, the PV system was treated as a steady power source, assuming sufficient energy storage to maintain constant operating conditions. The PV-generated electrical energy supports the pumping, heating, and cooling requirements of the DCMD subsystem, in addition to the operation of the PEM electrolyzer. It is noteworthy that the PEMWE system requires a direct current (DC), whereas the components of the DCMD subsystem operate with an alternating current. Therefore, appropriate power-conditioning units, including a DC/DC converter and an inverter, are required.

2.2. Modeling of the integrated system. The DCMD module has a flat-sheet membrane configuration[20]. The DCMD model assumes steady-state operation; uniform flow distribution; fully developed flow for heat and mass transfer analysis; negligible heat losses to the surroundings; only water vapor permeating the membrane (100% salt rejection); no membrane fouling, wetting, scaling, or degradation; constant feed salinity (maintained via makeup water); operation at atmospheric pressure; and constant feed and permeate inlet temperatures (maintained by the heater and chiller). The PEM electrolyzer model is based on standard literature assumptions[21] and additional simplifications. The system is assumed to operate in steady state at a uniform stack temperature. The stack is represented by identical cells connected in series, and the pressure effects are neglected, with the operation assumed to be under atmospheric conditions. Heat loss to the surroundings is considered to occur through natural convection from the endplates, with insulation applied to the sides of the electrolyzer[22]. Cathode activation losses are neglected, and the membrane is assumed to be fully hydrated, with its conductivity dependent only on temperature. For system validation, each subsystem was validated individually against experimental data from

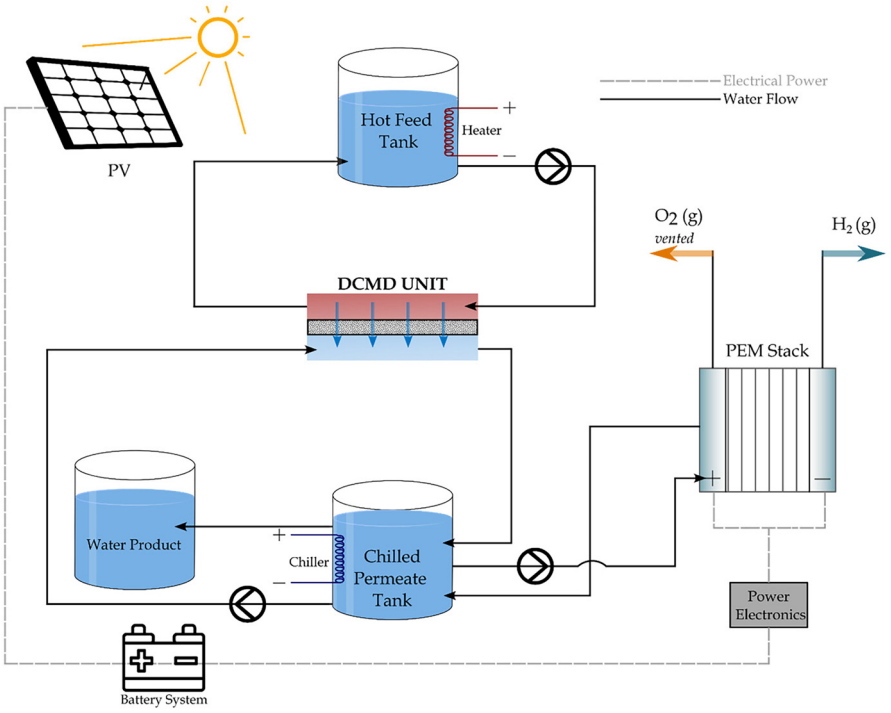


Figure 1. Schematic of DCMD–PEMWE System Integration

the literature because data for a similar integrated system are not available in the literature.

2.2.1. DCMD model. The DCMD model describes coupled heat and mass transfer across the membrane under steady-state conditions. The model can be divided into two integral parts[20], heat and mass transfers. Heat transfer in DCMD occurs in three regions[20]: Convection heat transfer occurs on both sides of the membrane between the bulk fluid and membrane surface. Conductive and evaporative heat transfers occur through the membrane. The convective heat flux from the feed stream to the membrane surface is governed by Newton's law of cooling[23]:

$$Q_f = h_f \left(T_{bf} - T_{mf}\right), \tag{1}$$

where Q_f is the heat flux from the feed side, h_f is the convective heat transfer coefficient at the feed side, and T_{bf} and T_{mf} are the bulk feed and membrane surface temperatures at the feed side, respectively. The heat carried by vapor transport is expressed as follows[24]:

$$Q_v = J_w \Delta H_v, \tag{2}$$

where J_w is the permeate mass flux and ΔH_v is the enthalpy of vaporization. The conductive heat flux,Q_c, through the membrane is expressed as follows[24]:

$$Q_c = \frac{k_m}{\delta}\left(T_{mf} - T_{mp}\right), \tag{3}$$

where k_m is the effective membrane thermal conductivity, δ is the membrane thickness, and T_{mp} is the membrane surface temperature at the permeate side. The total heat transfer across the membrane is expressed as follows:

$$Q_m = Q_c + Q_v. \tag{4}$$

On the permeate side, the convective heat transfer is expressed as follows:

$$Q_p = h_p \left(T_{mp} - T_{bp}\right). \tag{5}$$

Under steady-state conditions, the energy balance across the membrane is expressed as follows:

$$Q_p = Q_f = Q_m. \tag{6}$$

The convective heat transfer coefficient is calculated as follows:

$$h = \frac{Nu \times k}{D_h}, \tag{7}$$

where Nu is the Nusselt number, k is the thermal conductivity of the fluid, and D_h is the hydraulic diameter of the flow channel. The appropriate Nusselt number is selected based on laminar or turbulent flow characteristics[25]. Accounting for salinity, the permeate mass flux is governed by the pressure difference that arises from the temperature difference across the membrane and is expressed as follows[26]:

$$J_w = D_e \left(p^0_{wf} \times \gamma_{wf} \times x_{wf} - p^0_{wp}\right), \tag{8}$$

where J_w is the permeate mass flux, D_e is the effective diffusion coefficient[26], p^0_{wf} and p^0_{wp} are the vapor pressures at the feed and permeate membrane surfaces, respectively, γ_{wf} is the activity coefficient[27], and x_{wf} is the mole fraction of water in the feed. The vapor pressures are evaluated using the Antoine equation, as follows:

$$p^0_{w(f\ or\ p)} = \exp\left(23.1964 - \frac{3816.44}{T_{m(f\ or\ p)} - 46.13}\right). \tag{9}$$

2.2.2. PEMWE model. PEMWE produces hydrogen through the electrochemical splitting of water. Water is supplied

to the anode, where it is oxidized to generate oxygen, protons, and electrons. Protons are transported through the membrane to the cathode, whereas electrons flow through the external circuit. At the cathode, hydrogen is produced through a reduction reaction. This process is driven by an electrical potential applied across the electrodes. Figure 2 illustrates the overall process and the corresponding electrochemical half-reactions.

The PEM electrolyzer model can be divided into three interconnected models[21]: electrochemical, hydrogen production, and thermal. The electrochemical model determines the required stack voltage as a function of the operating current density and temperature. The hydrogen production model quantifies the molar flow rates of hydrogen production and water consumption based on Faraday's law. The thermal model accounts for heat generation within the stack and is used to evaluate the cooling requirements to maintain the stack at a specified operating temperature. The cell voltage can be represented as the sum of the reversible potential U_{rev}, the minimum theoretical voltage required to initiate the electrolysis reaction, and overpotentials $\eta_{activation}$ and η_{ohmic}, which represent the additional voltage required to overcome the losses in a PEM cell. The cell operating voltage (V_{cell}) is expressed as follows[21]:

$$V_{cell} = U_{rev} + \eta_{activation} + \eta_{ohmic}. \tag{10}$$

The reversible voltage is determined as a function of the temperature using an empirical relationship derived from the Nernst equation[28]. The activation overpotential accounts for the energy required to overcome the specific energy threshold associated with the evolution reactions occurring at the anode and cathode, as presented in Figure 2. Under the assumptions of the integrated system, only the anode overpotential is considered, as it dominates over the cathode overpotential owing to the more complex reaction kinetics at the anode, and is expressed as follows[21]:

$$\eta_{activation} = \frac{RT_{stack}}{\alpha z F} \ln\left(\frac{i}{i_{0,anode}}\right), \tag{11}$$

where i is the current density, which is the total current supplied to the system per unit area of PEM; $i_{0,anode}$ is the exchange current density at the anode, a value dependent on electrode material, surface morphology, and temperature that determines the reaction rate and required activation overpotential; α is the charge transfer coefficient, representing the fraction of overpotentials driving the oxidation and reduction reactions and typically assumed to be 0.5 under symmetric reaction conditions[21]; and z is the number of electrons involved in the reaction. The exchange current density temperature dependency is modeled using an Arrhenius-type relation[21].

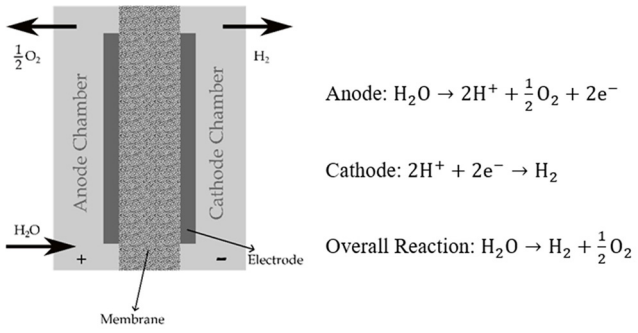


Figure 2. Electrolysis Process in PEM

Additionally, ohmic losses arise from the resistance to proton transport through the membrane (R_{ion}) and electronic resistance within the cell components ($R_{electronic}$). The membrane conductivity, σ, is modeled using an Arrhenius expression, where it is a function of temperature and the activation energy for proton transport, which represents the energy threshold that protons must overcome to move through the solid polymer membrane. As the temperature increases, the proton mobility within the membrane improves, leading to higher conductivity and reduced ionic resistance. The ionic resistance of the membrane is expressed as follows[21]:

$$R_{ion} = \frac{t_{membrane}}{\sigma}, \tag{12}$$

where $t_{membrane}$ is the membrane thickness. This expression highlights that thinner membranes and higher conductivity reduce resistive losses. The ohmic overpotential is calculated as follows[21]:

$$\eta_{ohmic} = (R_{electronic} + R_{ionic})\, i. \tag{13}$$

Electronic resistance can be obtained from measurements across the stack terminals under open-circuit conditions or can be neglected[21]; in this model, a constant value based on the literature was adopted. The total required stack power is calculated as follows[21]:

$$P_{stack} = (n_{cells}\, V_{cell})\, I, \tag{14}$$

where I is the total current, and n_{cells} is the number of cells in the stack. The hydrogen production model describes the generation rates of hydrogen, oxygen, and water consumption based on Faraday's law. The molar flow rates are expressed as follows[21]:

$$\dot{n}_{H_2} = \frac{n_{cells} I}{2F}\eta_F, \tag{15}$$

$$\dot{n}_{H_2O} = 1.25\frac{n_{cells} I}{2F}\eta_F, \tag{16}$$

where $\dot{n}_{H_2}$ and $\dot{n}_{H_2O}$ are the molar flow rates of hydrogen and consumed water, respectively, n_{cells} is the number of cells in the stack, F is Faraday's constant, and η_F is the Faradaic efficiency, representing the effective utilization of current for hydrogen production, typically ranging 0.96–0.99 in PEM electrolyzers. Finally, the thermal model accounts for heat generation within the electrolyzer and the associated heat losses and cooling requirements. The thermoneutral voltage is defined as the potential at which the heat generated through electrical energy equals the energy required for the electrolysis reaction and is obtained as follows[29]:

$$U_{th} = \frac{\Delta H_R}{zF}, \tag{17}$$

where ΔH_R is the reaction enthalpy. Although electrolysis is endothermic, a voltage higher than the thermoneutral voltage is required because of system inefficiencies. Consequently, the stack generates heat, which can be expressed as follows[21]:

$$Q_{gen} = n_{cells}\,(V_{cell} - U_{th})\, I_{total}. \tag{18}$$

The cooling requirement is calculated as follows:

$$Q_{cooling} = \dot{m}_{water} C_p \left(T_{out} - T_{in}\right), \tag{19}$$

where $\dot{m}_{water}$ is the water mass flow, C_p is the specific heat capacity, T_{out} and T_{in} are the outlet and inlet temperatures of the electrolyzer, respectively. This equation quantifies the cooling demand required to maintain a constant stack temperature under steady-state conditions. For the considered model, the PEM electrolyzer was represented using a simplified single-inlet, single-outlet water flow configuration, neglecting the phase separation and cathode-side recirculation.

2.2.3. System integration. As outlined in Section 2.1, the primary integration point between the DCMD and PEM subsystems is the permeate storage tank, which serves as a control volume by coupling the mass and energy flows of the desalination and electrolysis units. To evaluate the system performance, the net water production rate is defined as follows:

$$\dot{V}_{net} = \dot{V}_{DCMD} - \dot{V}_{PEM}, \tag{20}$$

where $\dot{V}_{DCMD}$ and $\dot{V}_{PEM}$ represent the DCMD water production and PEM water consumption rates, respectively. The net production rate is used to identify the operating conditions under which water production balances the electrolyzer demand. Additionally, the overall system efficiency is defined as follows:

$$\eta_{sys} = \frac{\left(\dot{n}_{H_2} \times HHV_{H_2}\right) + \left(\dot{m}_{net} \times \Delta H_v\right)}{P_{req}}, \tag{21}$$

where $\dot{n}_{H_2}$ is the molar hydrogen production rate, HHV_{H_2} is the higher heating value of hydrogen, $\dot{m}_{net}$ is the net water production, and ΔH_v is the enthalpy of vaporization. This definition accounts for the cogenerative nature of the system by including both the chemical energy of hydrogen and the thermal value of the produced water. The total system power requirement supplied by the PV panels is expressed as follows:

$$P = Q_{heating} + Q_{cooling} + P_{stack}, \tag{22}$$

where $Q_{heating}$ is the heating power for the DCMD feed, and $Q_{cooling}$ represents the total cooling power of the system.

3. MODEL VALIDATION

The developed models were solved using an Engineering Equation Solver and validated against experimental data available in the literature. The DCMD model was validated against the experimental data reported by Khalifa et al.[20], who conducted experiments using a flat-sheet PTFE membrane DCMD

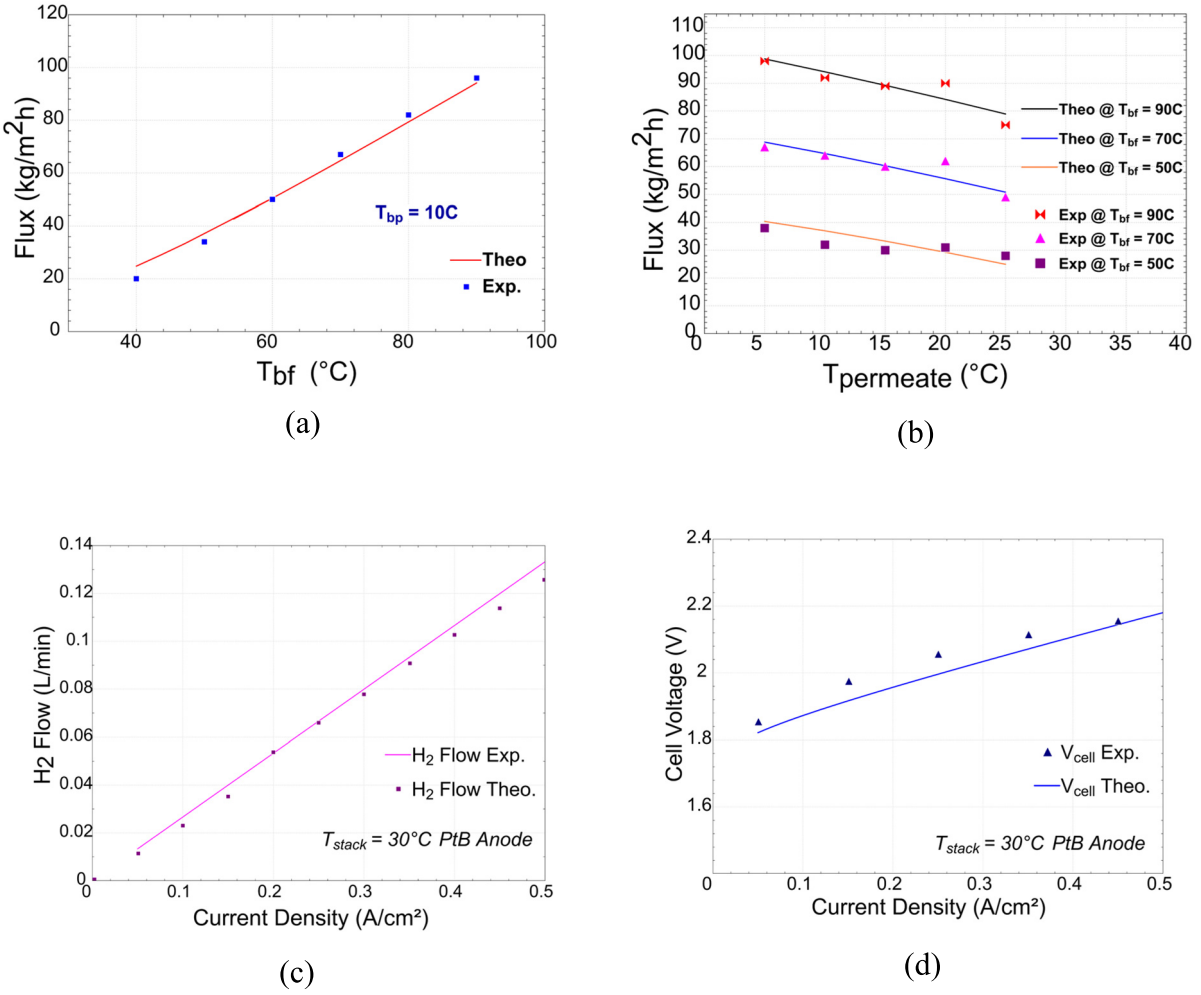


Figure 3. DCMD and PEMWE model validation: (a) DCMD validation with feed temperature; (b) DCMD validation with permeate temperature; (c) PEMWE validation for hydrogen production; and (d) PEMWE validation for cell voltage

module under different feed and permeate temperature conditions. The validation data are presented in Figures 3(a) and 3(b). The model-predicted results closely align with the experimental results, with the errors remaining below 10%. For the hydrogen production model, the I–V polarization curve was plotted and validated using the experimental data from Azam et al.[30] and the reference data from the literature[31–34]. Azam et al.[30] experimentally evaluated a 36 cm^2 single-cell PEM electrolyzer equipped with a Nafion 115 membrane and operated with deionized water. Multiple anode catalyst configurations were investigated; the validation presented in this work uses the experimental data corresponding to the PtB anode configuration. The correlation between the current density and hydrogen production was studied and validated, as shown in Figure 3(c), demonstrating a close alignment between the theoretical predictions and experimental data. Additionally, the effect of the current density on the voltage is presented in Figure 3(d), where an acceptable agreement is observed. The complete validation input data are provided in the Supplementary Material (Tables 1 and 2).

4. RESULTS AND DISCUSSION

Two operational scenarios were considered: (A) DCMD water production was completely utilized by the PEMWE for hydrogen production, corresponding to zero water demand, and (B) DCMD was operated for both freshwater demand and hydrogen production. Table 1 summarizes the model's input data used to analyze scenarios (A) and (B). In Scenario (A), a membrane area of 200 cm^2 was employed, whereas in Scenario (B) an area of 0.5 m^2 was used to provide more water for the demand. For the proposed system, the PEMWE size was that of a 1–2 kW electrolyzer, according to the chosen operating current density.

4.1. Operation Scenario (A). For Scenario (A), the system operation and water production were designed to maintain a constant water mass in the permeate tank such that the water production from the DCMD matched the water consumption of the PEM electrolyzer with zero water demand. Figure 4(a) compares the DCMD productivity at different feed temperatures with the PEMWE water consumption. The intersection points represent the maximum operating limits at each temperature, indicating that the system can operate safely at current densities equal to or below these values. Higher feed temperatures result in increased productivity, shifting the intersection point of the consumption curve to higher current densities. The water consumption of PEMWE is directly proportional to the current density. Figure 4(b) illustrates the mass flow rates of the reactants and products, showing the hydrogen and oxygen production along with the corresponding water consumption, consistent with the stoichiometric ratios. The net water flow rate is also shown, which is defined as the difference between DCMD production and PEMWE consumption. At zero current density (PEMWE inactive), the system exhibited a maximum net production of 0.6976 kg/h. As the current density increased, water consumption increased linearly, resulting in a decrease in net production until it reached zero. This point defines the maximum allowable operating current density, $i_{max} = 2.29$ A/cm^2, beyond which the system consumption exceeds productivity.

Table 1. *Input parameters and values used in the model*

DCMD Parameters	Value
Membrane thickness	7 µm
Pore diameter	0.45 µm
Membrane porosity	0.80
Channel width	0.024 m
Channel height	0.005 m
Channel length	0.066 m
Feed temperature	60 °C
Permeate temperature	25 °C
Feed pressure	101325 Pa
Permeate pressure	101325 Pa
Feed flow rate	1.533 L/min (A), 36.8 L/min (B)
Permeate flow rate	1.217 L/min (A), 29.2 L/min (B)
Salinity	40 g/L
PEMWE parameters	Value
Number of cells	15
Active cell area	50 cm^2
Membrane thickness	127 µm
Membrane conductivity (ref)	0.033 S/cm
Stack temperature	50 °C
Exchange current density (anode)	1.0×10^{-9} A/cm^2
Activation energy (anode)	68 kJ/mol
Electronic resistance	0.3 Ω · cm^2
Faradaic efficiency	96%
Stack current	30 A

Figure 5 presents the influence of the key operating parameters on the system efficiency, as indicated by Eq. 21. Figures 5(a)–(c) are generated by enforcing a zero net water demand condition, while varying the stack temperature between 50 and 80 °C. The corresponding current density satisfying this condition was determined for each temperature. As shown in Figure 5(a), the system efficiency decreases with increasing current density owing to an increase in the overpotentials, leading to higher energy consumption. Figure 5(b) shows that the efficiency improves with increasing stack temperature, as higher operation temperatures enhance the reaction kinetics and membrane conductivity, reducing the required cell voltage. Figure 5(c) shows that increasing the feed temperature increases DCMD productivity, requiring higher current densities and reducing efficiency. Higher feed temperatures increase the heating demand, whereas lower permeate temperatures increase the cooling requirements, further lowering efficiency. Figure 5(d) shows that PEMWE cell voltage decreases with temperature owing to improved kinetics and conductivity but increases with current density owing to polarization losses. Overall, higher stack temperatures and favorable DCMD thermal conditions enhance the efficiency, whereas high current densities reduce it.

4.2. Operation Scenario (B). In this scenario, a larger membrane area (0.5 m^2) was considered to secure freshwater production output in addition to the desired hydrogen production. Figure 6(a) presents the variation in system efficiency with the bulk feed temperature for different permeate temperatures. An overall increasing trend is observed, indicating that higher feed temperatures improve the system efficiency because of the significant increase in water production at elevated feed temperatures, which offsets the additional thermal energy required

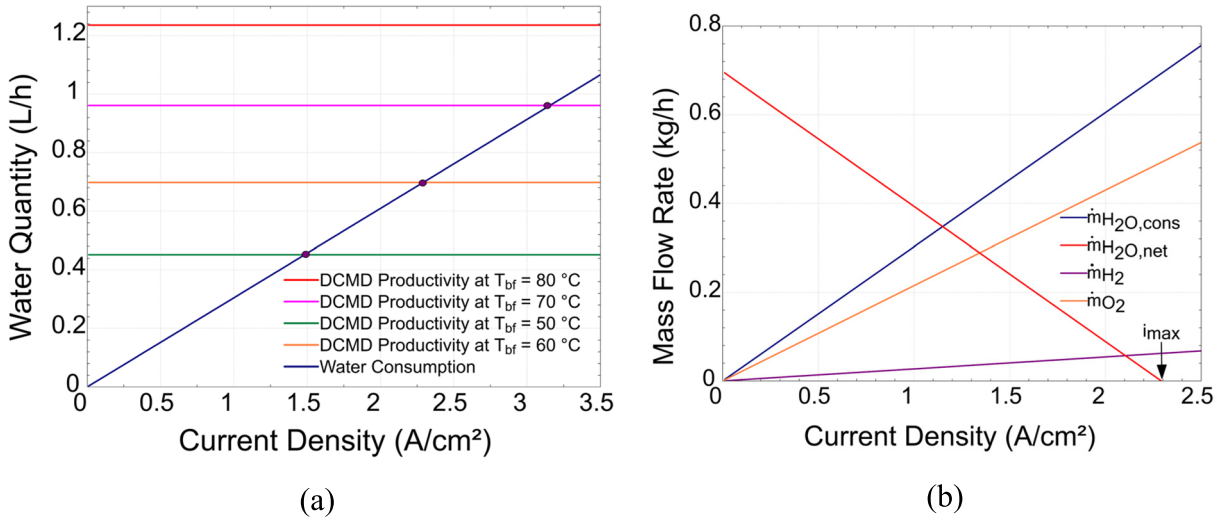


Figure 4. Water supply, demand, and production of the integrated DCMD-PEMWE system: (a) DCMD water production at different feed temperatures compared with PEMWE consumption; and (b) mass flow rates of water consumption, net balance, and electrolysis products versus current density

for heating. At lower feed temperatures, a deviation is observed where the curve corresponding to $T_{perm} = 30$ °C falls below those of 20 and 25 °C. This can be explained by the reduced temperature difference across the membrane (ΔT), which limits vapor transport and flux. Figure 6(b) shows the percentage of useful water products after accounting for PEMWE consumption. More than 95% of the produced water remains available as a useful output, indicating that PEMWE water consumption is minimal compared with DCMD production. This demonstrates the effectiveness of the system for the simultaneous cogeneration of water and hydrogen.

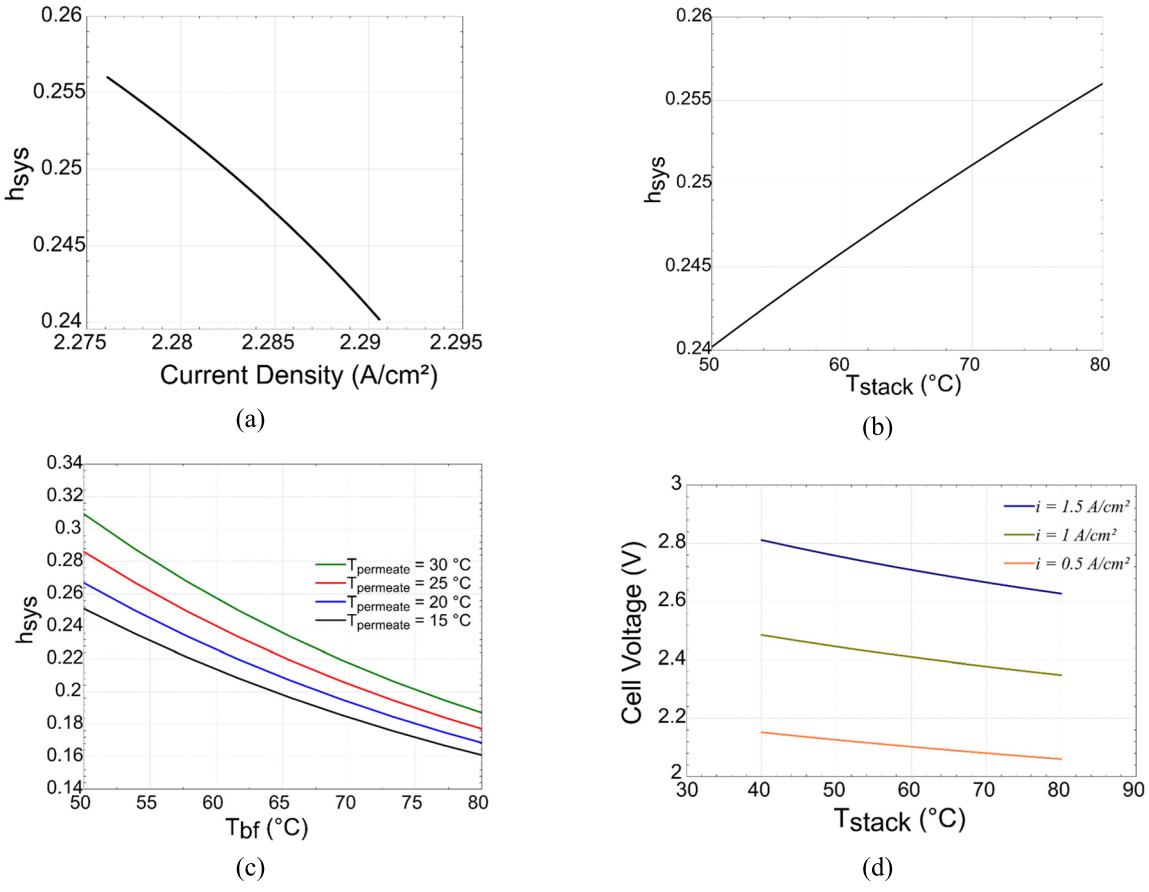


Figure 5. Influence of operating parameters on system efficiency: (a) variation with current density; (b) variation with stack temperature; (c) variation with feed and permeate temperatures; and (d) PEMWE cell voltage as a function of stack temperature at different current densities

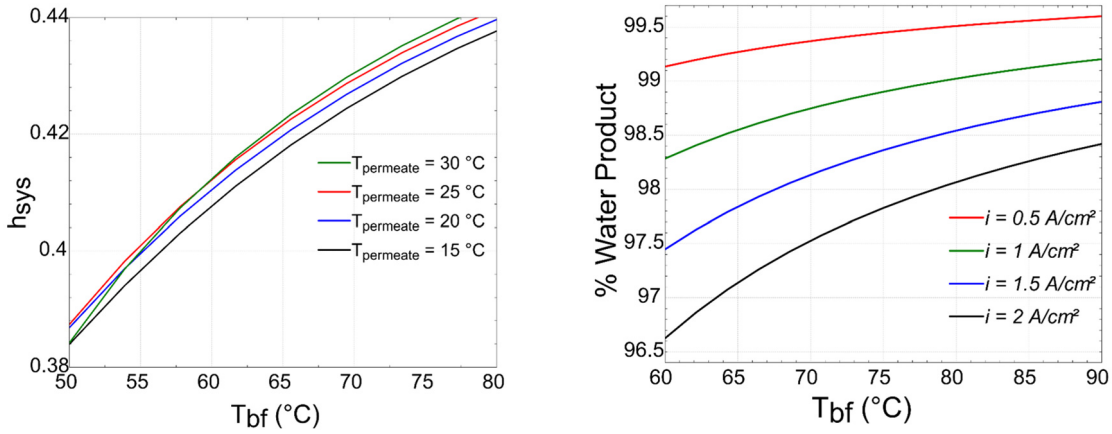


Figure 6. Effects of feed water temperature on (a) integrated system efficiency and (b) % water consumed by the PEM relative to DCMD desalinated water production

Distinguishing between PEMWE water consumption and the overall water requirement of the PEM system is important. Although the electrochemical consumption is relatively low, practical PEM systems require significantly higher flow rates for thermal management and cooling. Therefore, an initial freshwater reservoir is necessary to sustain the system operation. Figure 7 shows the required system circulation flow rate as a function of stack temperature. The flow rate decreases with increasing stack temperature owing to the improved system efficiency, which reduces the heat generation and cooling demand. Additionally, the effect of current density is consistent with previous observations, where higher current densities lead to decreased efficiency and, consequently, higher circulation requirements.

4.3. Study Limitations. The present study is subject to several limitations. Although each subsystem was individually validated against published experimental data, the performance of the integrated DCMD–PEMWE system remains theoretical until validated experimentally. The PEM electrolyzer model relies on literature-based electrochemical parameters, such as the exchange current density and proton transport properties, which may require further calibration for specific electrolyzer configurations. Additionally, the PEM cooling loop was represented using a simplified water circulation model that does not explicitly account for detailed recirculation strategies employed in practical systems. Finally, the present model assumes a prescribed inlet and outlet water temperature for the PEM electrolyzer, from which the required circulation flow rate is calculated, without explicitly modeling an electrolyzer feedwater preheating process. Most PEM electrolyzer studies employ preheated inlet water and sufficiently high circulation flow rates to maintain a small inlet-to-outlet temperature rise and prevent system degradation. However, experimental investigations have shown that large inlet-to-outlet temperature rises may occur under low-flow operating conditions. For example, Du et al.[35] reported temperature rises exceeding 30 °C under these conditions. Future work should investigate thermal management strategies that reduce the inlet-to-outlet water temperature rise, as large temperature rises have been reported to compromise membrane durability[35].

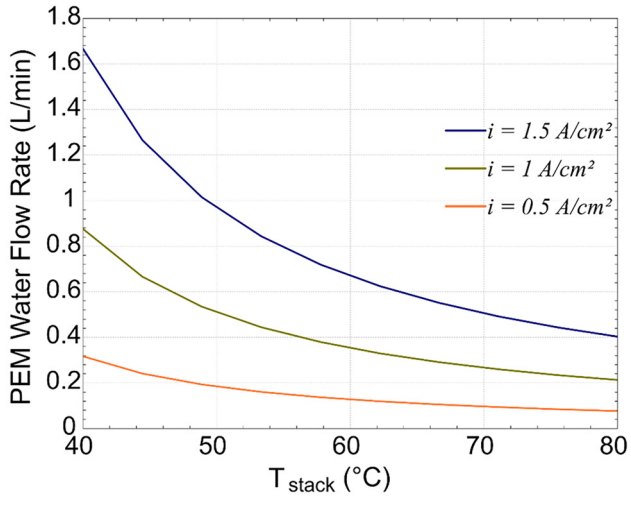


Figure 7. Required system circulation flow rate as a function of stack temperature

5. CONCLUSION

In this study, a steady-state theoretical model of an integrated DCMD–PEMWE system was used to evaluate the feasibility of coupled freshwater and hydrogen production. The results indicate that system operation is primarily governed by the balance between DCMD water production and PEMWE water consumption, defining a maximum sustainable current density of 2.29 A/cm^2 for the first considered configuration. Increasing the feed temperature enhanced the DCMD productivity and extended the feasible operating range, whereas higher current densities reduced the efficiency owing to increased overpotentials and cooling requirements. Conversely, higher stack temperatures (50–80 °C) improved system efficiency by lowering cell voltage and heat generation. In the cogeneration scenario, increasing the membrane area enabled simultaneous hydrogen and freshwater production, with more than 95% of the produced water remaining available as useful output. The analysis also showed that the PEMWE water circulation requirements are dominated by thermal management rather than electrochemical consumption,

highlighting the importance of cooling considerations in system design. Overall, this study confirms the viability of DCMD–PEMWE integration and provides a baseline for optimizing and analyzing water–hydrogen cogeneration systems. Future work should focus on dynamic modeling, renewable or waste-heat integration, system optimization, and experimental validation.

AFFILIATIONS AND AUTHOR DETAILS

Undergraduate Author

Alaa M. Ahmed – *Department of Mechanical Engineering, King Fahd University of Petroleum & Minerals, Dhahran 31261, Saudi Arabia*; 0009-0005-9396-6449
Email: s202332770@kfupm.edu.sa

Corresponding Author

Atia Khalifa – *Research Mentor, Professor, Department of Mechanical Engineering, King Fahd University of Petroleum & Minerals, Dhahran 31261, Saudi Arabia*; 0000-0002-1271-1497
Email: akhalifa@kfupm.edu.sa

ACKNOWLEDGEMENTS

The authors would like to acknowledge the support provided by the Department of Mechanical Engineering and the Interdisciplinary Research Center of Sustainable Energy Systems at King Fahd University of Petroleum and Minerals.

REFERENCES

(1) Bhuiyan, M. M. H. & Siddique, Z. Hydrogen as an alternative fuel: a comprehensive review of challenges and opportunities in production, storage, and transportation. *Int. J. Hydrogen Energy* **102**, 1026–1044 (2025).

(2) IEA. *Global Hydrogen Review 2025*. (International Energy Agency, 2025).

(3) Nasser, M., Megahed, T. F., Ookawara, S. & Hassan, H. A review of water electrolysis–based systems for hydrogen production using hybrid/solar/wind energy systems. *Environ. Sci. Pollut. Res.***29**, 86994–87018 (2022).

(4) Becker, H. *et al.* Impact of impurities on water electrolysis: a review. *Sustainable Energy and Fuels* **7**, 1565–1603 (2023).

(5) Kıstı, M. *et al.* Recent advances in polymer electrolyte membrane water electrolyzer stack development studies: a review. *ACS Omega* **10**, 9824–9853 (2025).

(6) Simoes, S. G. *et al.* Water availability and water usage solutions for electrolysis in hydrogen production. *J. Clean. Prod.* **315**, 128124 (2021).

(7) Bianco, E., Luo, T. & Nagpal, D. *Water for Hydrogen Production*. (International Renewable Energy Agency, 2023).

(8) Xie, H. *et al.* A membrane-based seawater electrolyser for hydrogen generation. *Nature* **612**, 673–678 (2022).

(9) Winter, L. R. *et al.* Mining nontraditional water sources for a distributed hydrogen economy. *Environ. Sci. Technol.* **56**, 10577–10585 (2022).

(10) Kumar, P., Date, A., Mahmood, N., Kumar Das, R. & Shabani, B. Freshwater supply for hydrogen production: an underestimated challenge. *Int. J. Hydrogen Energy* **78**, 202–217 (2024).

(11) Seyed Sabour, S. M. J. & Ghorashi, B. A comprehensive review of major water desalination techniques and mineral extraction from saline water. *Sep. Purif. Technol.* **349**, 127913 (2024).

(12) Katakam, V. S. S. & Bahadur, V. Reverse osmosis-based water treatment for green hydrogen production. *Desalination* **581**, 117588 (2024).

(13) Ellersdorfer, P., Omar, A., Taylor, R. A., Daiyan, R. & Leslie, G. Multi-effect distillation: a sustainable option to large-scale green hydrogen production using solar energy. *Int. J. Hydrogen Energy* **48**, 31491–31505 (2023).

(14) Kianfard, H., Khalilarya, S. & Jafarmadar, S. Exergy and exergoeconomic evaluation of hydrogen and distilled water production via combination of PEM electrolyzer, RO desalination unit and geothermal driven dual fluid ORC. *Energy Convers. Manag.* **177**, 339–349 (2018).

(15) Liang, Y. Y. & Shahabuddin, M. Production of green hydrogen from desalinated water using membranes: a review. *Desalination* **614**, 119200 (2025).

(16) Arthur, T., Millar, G. J. & Love, J. Thermal management of water electrolysis using membrane distillation to produce pure water for hydrogen production. *J. Water Process Eng.* **67**, 106255 (2024).

(17) Xu, X., Zhao, Z., Song, C., Xu, L. & Zhang, W. Seawater membrane distillation coupled with alkaline water electrolysis for hydrogen production: parameter influence and techno-economic analysis. *Membranes* **15**, 60 (2025).

(18) Schwantes, R. *et al.* Thermally driven ultrapure water production for water electrolysis – a techno-economic analysis of membrane distillation. *Desalination* **608**, 118848 (2025).

(19) Zhao, W. *et al.* Membrane distillation for producing ultra-pure water for PEM electrolysis. *Int. J. Hydrogen Energy* **99**, 232–240 (2025).

(20) Khalifa, A., Ahmad, H., Antar, M., Laoui, T. & Khayet, M. Experimental and theoretical investigations on water desalination using direct contact membrane distillation. *Desalination* **404**, 22–34 (2017).

(21) García-Valverde, R., Espinosa, N. & Urbina, A. Simple PEM water electrolyser model and experimental validation. *Int. J. Hydrogen Energy* **37**, 1927–1938 (2012).

(22) Eichner, B. J., Amiri, M. N., Burheim, O. S. & Lamb, J. J. 2D simulation of temperature distribution within large-scale PEM electrolysis stack based on thermal conductivity measurements. *Front. Chem. Eng.* **6**, 1384772 (2024).

(23) Ho, C. D., Huang, C. H., Tsai, F. C. & Chen, W. T. Performance improvement on distillate flux of countercurrent-flow direct contact membrane distillation systems. *Desalination* **338**, 26–32 (2014).

(24) Alkhudhiri, A., Darwish, N. & Hilal, N. Membrane distillation: a comprehensive review. *Desalination* **287**, 2–18 (2012).

(25) Srisurichan, S., Jiraratananon, R. & Fane, A. G. Mass transfer mechanisms and transport resistances in direct contact membrane distillation process. *J. Memb. Sci.* **277**, 186–194 (2006).

(26) Essalhi, M. & Khayet, M. Self-sustained webs of polyvinylidene fluoride electrospun nanofibers at different electrospinning times: 2. Theoretical analysis, polarization effects and thermal efficiency. *J. Memb. Sci.* **433**, 180–191 (2013).

(27) Khayet, M. & Matsuura, T. *Membrane Distillation: Principles and Applications*. (Elsevier, 2011).

(28) Roy, A., Watson, S. & Infield, D. Comparison of electrical energy efficiency of atmospheric and high-pressure electrolysers. *Int. J. Hydrogen Energy* **31**, 1964–1979 (2006).

(29) Bessarabov, D., Wang, H., Li, H. & Zhao, N. *PEM Electrolysis for Hydrogen Production : Principles and Applications*. (CRC Press, 2016).

(30) Noor Azam, A. M. *et al.* Parametric study and electrocatalyst of polymer electrolyte membrane (PEM) electrolysis performance. *Polymers* **15**, 560 (2023).

(31) Carmo, M., Fritz, D. L., Mergel, J. & Stolten, D. A comprehensive review on PEM water electrolysis. *Int. J. Hydrogen Energy* **38**, 4901–4934 (2013).

(32) Kroschel, M., Bonakdarpour, A., Kwan, J. T. H., Strasser, P. & Wilkinson, D. P. Analysis of oxygen evolving catalyst coated membranes with different current collectors using a new modified rotating disk electrode technique. *Electrochim. Acta* **317**, 722–736 (2019).

(33) Yodwong, B. *et al.* Faraday's efficiency modeling of a proton exchange membrane electrolyzer based on experimental data. *Energies* **13**, 4792 (2020).

(34) Silva, R. F., De Francesco, M. & Pozio, A. Tangential and normal conductivities of Nafion®membranes used in polymer electrolyte fuel cells. *J. Power Sources* **134**, 18–26 (2004).

(35) Du, T., Wang, C., Ma, H., Xu, Y. & Li, Y. Experimental investigation on the effects of water flow rates and wind speeds on the temperature and performance of PEM electrolyzer stacks. *Energy* **334**, 137694 (2025).